ACS OMEGA

Ag-Vanadates/GO Nanocomposites by Aerosol-Assisted Spray Pyrolysis: Preparation and Structural and Electrochemical Characterization of a Versatile Material
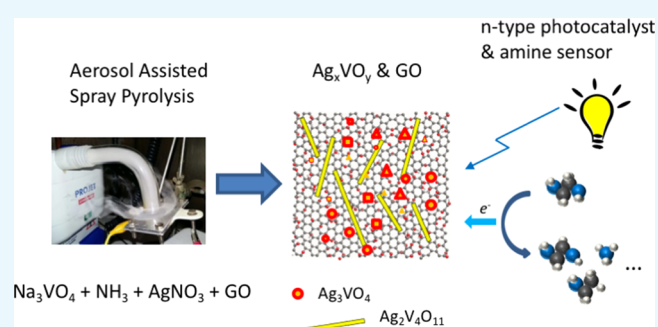
Jian Zheng,[†,∥] Laura Calvillo,[†] Carlos Valero-Vidal,[‡] Carla Marega,[†] Pandiaraj Sekar,[†] Shuang Shuang,[†,§] Leonardo Girardi,[†] Stefano Agnoli,[†] Gian Andrea Rizzi,*[,†] and Gaetano Granozzi[†]

[†]Dipartimento di Scienze Chimiche, Università degli Studi di Padova, Via Marzolo 1, 35131 Padova, Italy

[‡]Advanced Light Source (ALS), Joint Center for Energy Storage Research (JCESR), Lawrence Berkeley National Laboratory, 1 Cyclotron Road, Berkeley, California 94729, United States

[§]State Key Laboratory of New Ceramics and Fine Processing, School of Materials Science and Engineering, Tsinghua University, Beijing 100084, China

ABSTRACT: In this article, we describe the deposition by aerosol-assisted spray pyrolysis of different types of silver vanadate nanocomposites with and without graphene oxide (GO) on different substrates (carbon paper (CP) and fluorine-doped tin oxide (FTO)). When deposited on CP, different amounts of GO were added to the Ag and V precursor solution to study the effect of GO on the physicochemical properties of the resulting Ag-vanadate. It is shown that the addition of GO leads mainly to the formation of nanoparticles of the $Ag_2V_4O_{11}$ phase, whereas $Ag_2V_4O_{11}$ and Ag_3VO_4 are obtained without the addition of GO. The morphology and chemical properties of the composites were determined by scanning and transmission electron microscopies, X-ray diffraction, X-ray photoemission spectroscopy, and UV−visible and Raman spectroscopies. In addition, the photoelectrochemical (PEC) properties of such composites were studied by CV, linear sweep voltammetry, and electrochemical impedance spectroscopy. The ideal Ag_xVO_y and GO ratio was optimized for obtaining higher photocurrent values and a good stability. The results showed that the presence of GO improves the electrical conductivity of the catalyst layer as well as the electron injection from the oxide to the electrode surface. The deposition of pure $Ag_2V_4O_{11}$ on FTO does not lead to samples with stable PEC performances. Samples grown on CP supports showed an efficient electrochemical detection of small amounts of ethylenediamine in water solution.

INTRODUCTION

Silver vanadates, especially in the form of α-Ag_3VO_4 and $AgVO_3$, are photocatalysts characterized by a sufficiently large band gap (ca. 2.0−2.2 eV[1−8]), potentially stable at water oxidation potentials due to the high oxidation state of V and the monovalent preference of Ag. Other Ag-vanadates, like $Ag_2V_4O_{11}$, have been studied and used as a cathode material in Li-ion batteries[9] and, more recently, as active materials in gas sensing devices. In particular, nanoribbons of $Ag_2V_4O_{11}$ were used in the detection of amines and alcohols in the gas phase with good sensitivity.[10] Nevertheless, up to now, the studies of these materials as photocatalysts have focused on particles dispersed in water, and most of them have addressed dye degradation. The particles are usually synthesized by hydrothermal methods or simple precipitation. Nevertheless, these experimental conditions (samples in the powder form) make difficult the accurate measurement of important quantities such as flat-band potential, photocurrent onset potential, and the photocurrent as a function of potential. α-Ag_3VO_4 thin films, like other vanadates, can be difficult to prepare by standard

growth techniques (CVD and sputtering, for example, because of the difficulties in obtaining a definite stoichiometry), but very recently a study by Chemelewski et al. described the successive ionic layer adsorption and reaction (SILAR) growth of α-Ag_3VO_4 thin films and their characterization for photo-electrochemical water splitting (PEC-WS).[11] The results of this study demonstrate that the as-grown material is characterized by p-type conductivity and therefore cannot be used as a photoanode. However, an annealing treatment in air up to 300 °C introduces n-type conductivity. Unfortunately, the resulting n-type behavior is unstable under photocatalytic water oxidation conditions, so that the photocurrent continuously decreases with a corresponding anodic shift of the flat-band potential. The authors interpreted this behavior to be due to the removal of oxygen vacancies by photo-oxidation. This hypothetical self-oxidation is also in agreement with the

evidence that hole scavengers are not able to increase the measured photocurrent. The conclusion of this study was that, although the results are not promising for the outlook of α-Ag_3VO_4 as a PEC-WS material per se, its low band gap still makes it interesting for developing nanosystems characterized by a more efficient charge extraction by further nanostructuring. This statement and the lack in the literature of methods for preparing controlled nanostructured thin films led us to investigate the use of aerosol-assisted spray pyrolysis as an alternative, easy, and highly scalable technique to deposit Ag-vanadates (Ag_xVO_y) on conductive substrates, either conventional carbon materials or transparent conductive oxides (such as fluorine-doped tin oxide (FTO)), to improve the photocurrent stability and charge extraction. Although probably not suitable as PEC-WS materials yet, Ag-vanadates are attractive materials for the sensing of organics in a water solution taking advantage of their n-type conductivity that allows their use as photoanodes enhancing the detection sensitivity as already done in the case of TiO_2 thin films coupled with Cu_2O nanoparticles.[12] Moreover, the aerosol-assisted spray pyrolysis allows depositing a large variety of nanocomposite materials containing graphene oxide (GO) or reduced GO by a simple "one-pot" procedure. The rationale behind the addition of this second component lies in the possibility to improve the electrical contact among the oxide particles with the substrate, thus enhancing the injection of electrons on the electrode surface and therefore the PEC performances. Also, the presence of GO helps to obtain nanocomposites with a high surface area, by increasing the number of nucleation sites, acting as a sort of "fishing net" configuration[13] and eventually inducing the formation of different crystal phases. We used a precursor solution (VO_4^{3-} and Ag^+) in which Ag^+ ions are kept solvated by complexation with NH_3. The consequent alkaline pH also allows the stabilization of GO sheets forming a stable suspension. We have deposited Ag_xVO_y NPs by the aerosol-assisted method with different amounts of GO on a carbon paper (CP) and on an FTO glass. After the characterization of the materials by Raman spectroscopy, X-ray photoemission spectroscopy (XPS), wide-angle X-ray diffraction (WAXD), transmission electron microscopy (TEM), and scanning electron microscopy (SEM) measurements, we have verified that when GO is added to the mixture the main phase is actually $Ag_2V_4O_{11}$. We have tested these electrodes as photoanodes under visible light in $KHCO_3$ solution, and, at variance with the results obtained on the films deposited by SILAR on FTO,[11] we found a rather stable photocurrent for pure and Ag_xVO_y&GO composite materials on the CP support. Moreover, the presence Ag^+ ions in these materials makes them interesting candidates for the electrochemical detection of ammines.

■ RESULTS AND DISCUSSION

Material Characterization. In Figure 1, we report the SEM images of the deposits on CP obtained from pure Ag_xVO_y solution and Ag_xVO_y&GO 0.75 mg/mL. In the former case, it is well evident (Figure 1a) that the carbon fibers of the CP are coated with particles of very different shapes and sizes, whereas in the latter (Figure 1b,c) the particles are apparently smaller and more uniformly distributed. As evident from Figure 1b,c, the GO sheets are coating some areas of the carbon fibers like a "blanket". In Figure 1c, the typical wrinkles of GO sheets are also clearly visible. In Figure 1d, the morphology of the deposit obtained on the FTO glass is shown. The particles have a rather
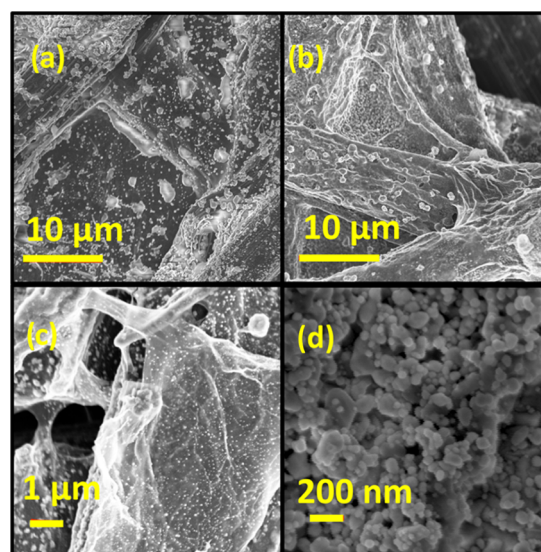

Figure 1. SEM images of the deposits on CP obtained from precursor solutions containing pure Ag_xVO_y (a) and Ag_xVO_y&GO 0.75 mg/mL (b). (c) Close-up view of the deposit from Ag_xVO_y&GO 0.75 mg/mL. (d) Morphology of the deposit obtained on FTO.

large size distribution (30−200 nm) with spherical particles growing on platelet-like larger crystals.

Figure 2 shows the results from XPS and WAXD measurements on the Ag_xVO_y&GO 0.75 mg/mL sample. The V 2p signals together with the O 1s peak are reported in Figure 2a. The V $2p_{3/2}$ signal is found, as expected, at 517.6 eV (V^{+5}), and no other component is present.[14,15] The O 1s $K\alpha_{3,4}$ satellite is also visible in the fitted spectra at about 522.4 eV. The O 1s peak (Figure 2a), instead, can be fitted with at least two components: the main one at 530.6 eV, corresponding to V−O bonds,[15] and the component at about 532.5 eV, which can be assigned to −OH and −COOH groups in GO and adsorbed water molecules. Because the O 1s peak of GO is also characterized by a main component at 530.5 eV, it is not possible (spectra not reported) to calculate the accurate stoichiometry (V/O ratio). In any case, if only the first O 1s component is considered, the resulting stoichiometry would be $VO_{3.5}$. However, the Ag MNN Auger peak (Figure 2b) shows, very clearly, the presence of both Ag^+ and metallic Ag. The fitting of the Ag MNN peak allows us to estimate the Ag^+/Ag ratio[16] (1:1), and consequently, the Ag^+/V ratio in the vanadate was found to be 0.5. The presence of metallic Ag is also verified by WAXD (Figure 2c):[19] the WAXD data show the presence of metallic Ag, Ag_3VO_4, and $Ag_2V_4O_{11}$. The presence of the peak at $2\theta = 29.4°$ is clearly attributable to the presence of $Ag_2V_4O_{11}$[17] (see also Raman spectra discussion below), whose structure is reported in Figure 2d. This peak should correspond to reflection from the $(\overline{2}03)$ planes, which is particularly evident in the case of $Ag_2V_4O_{11}$ prepared at alkaline pH, as in our case.[10,18] The intense peaks at $2\theta = 38.1$ and $44.3°$ confirm the presence of metallic Ag. It is noteworthy that in the case of the deposit obtained without GO, the peaks at $2\theta = 31$ and $32.4°$, which can be attributed to Ag_3VO_4, are more intense, indicating that the presence of GO leads to a higher $Ag_2V_4O_{11}/Ag_3VO_4$ ratio. To obtain the weight ratio of the different phases, we applied the quantitative analysis of the diffraction patterns of powder mixtures[19] that allows obtaining, considering the different absorption coefficients of each phase, the corresponding fraction by weight. To achieve greater accuracy, we
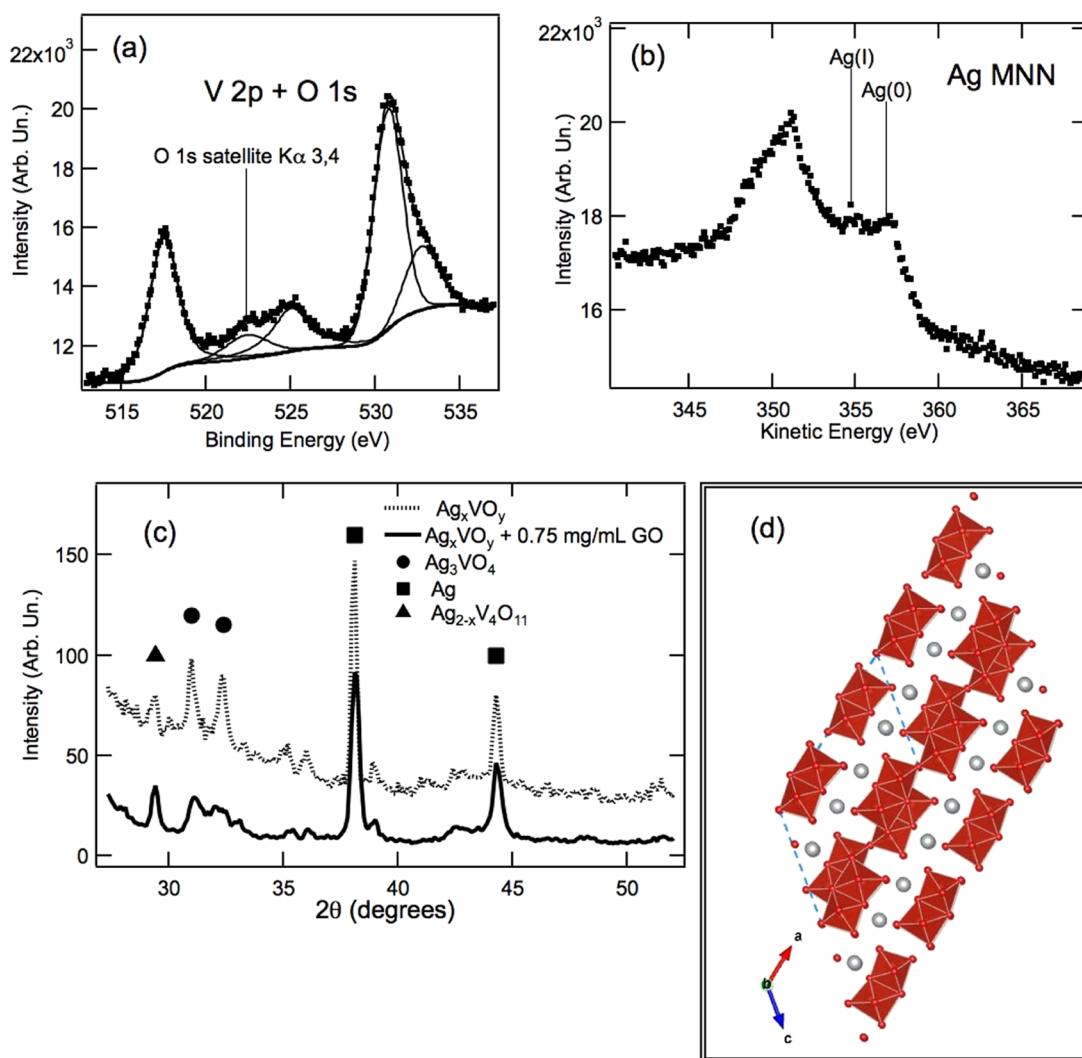
Figure 2. XPS and WAXD data of the deposits on CP obtained from the precursor solution containing Ag_xVO_y and Ag_xVO_y&GO 0.75 mg/mL. (a) V 2p and O 1s peaks. (b) Ag MNN Auger peak. (c) WAXD spectra. (d) Structure of $Ag_2V_4O_{11}$ (101) (type I). Oxygen atoms forming highly distorted octahedra around V^{5+} ions are clearly visible. Ag ions are represented in gray.

proceeded to the deconvolution of the peaks, by the application of the least-squares fit elaborated by Hindeleh and Johnson[20] and to the determination of the intensity, calculated as the area subtended by each peak. The results of this analysis are given in Table 1.

Deposits obtained on FTO, after annealing at 250 °C for 1 h, show only the presence of the $Ag_2V_4O_{11}$ phase, suggesting that this substrate favors the formation of such phases.

Table 1. Weight Ratios between $Ag_2V_4O_{11}$, Ag_3VO_4 and Ag Phases from XRD Analysis

phase	Ag_xVO_y	Ag_xVO_y & GO 0.75 mg/mL
$Ag_2V_4O_{11}$	18% (weight ratio)[a]	19%
Ag_3VO_4	37%	14%
Ag	45%	67%

[a]The differences between the amounts of phases measured by XRD and the results of XPS and Raman measurements can be due to the way in which the sample for XRD measurements was collected: each powder sample was collected by scraping the surface of the CP substrates. In this way, the phase that was more strongly anchored to the substrate was underestimated.

The presence of the $Ag_2V_4O_{11}$ as the main component is confirmed by TEM images. In fact, as reported in the literature, $Ag_2V_4O_{11}$ crystals are commonly found with a nanostripe or needle shape, as can be clearly seen in the images reported in Figure 3.[10] In Figure 3b, the $Ag_2V_4O_{11}$ needles can be clearly seen together on a GO sheet with typical wrinkles. The same crystalline shape is also found in the sample without GO. The darker spots correspond to metallic Ag nanoparticles and Ag_3VO_4, whose presence is also confirmed in the UV−vis spectra obtained on FTO glass. In Figure 3c,d, we report the EDX maps together with the corresponding SEM images acquired on Ag_xVO_y and Ag_xVO_y&GO 0.75 mg/mL after electrochemical work. In the case of the material deposited without GO, it is evident that large needles and stripes are grown on the CP surface together with smaller particles. However, when the growth is performed with GO, the dimension of the particles is more uniform, and "worm-like" structures appear probably due to the presence of the thin GO blanket. The Ag/V atomic ratio (which includes metallic Ag) determined by EDX is 3:5 in the case of Ag_xVO_y and 1:1 for Ag_xVO_y&GO 0.75 mg/mL. The UV−visible spectra of Ag_xVO_y and Ag_xVO_y&GO 0.75 mg/mL, grown on FTO and presented
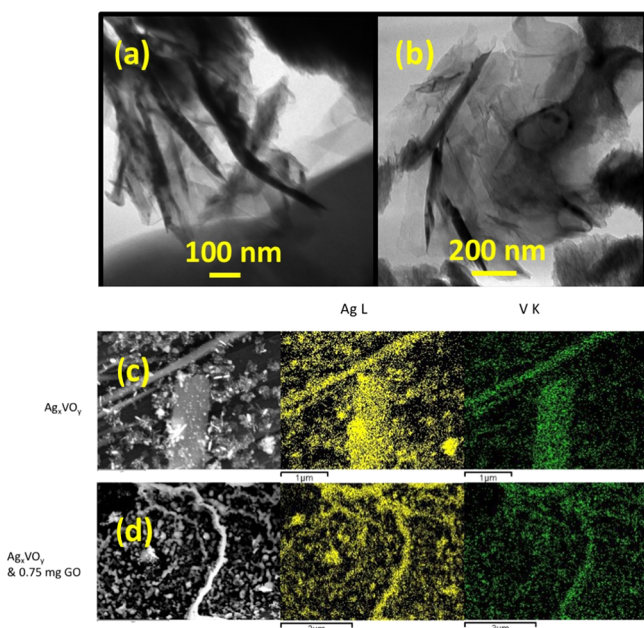
Figure 3. TEM images of Ag_xVO_y (a) and $Ag_xVO_y\&GO$ 0.75 mg/mL (b). $Ag_2V_4O_{11}$ crystals are characterized by the needle-like shape. Darker spots are due to residual Ag NPs or small amounts of Ag_3VO_4 (Ag_xVO_y sample). (c, d) SEM images and EDX element maps are reported. Large needle-like particles are visible for the Ag_xVO_y sample: smaller structures are found in the case of $Ag_xVO_y\&GO$ 0.75 mg/mL.

in Figure 4, are similar, and the main component, at about 430−450 nm, is overlapping with localized surface plasmon

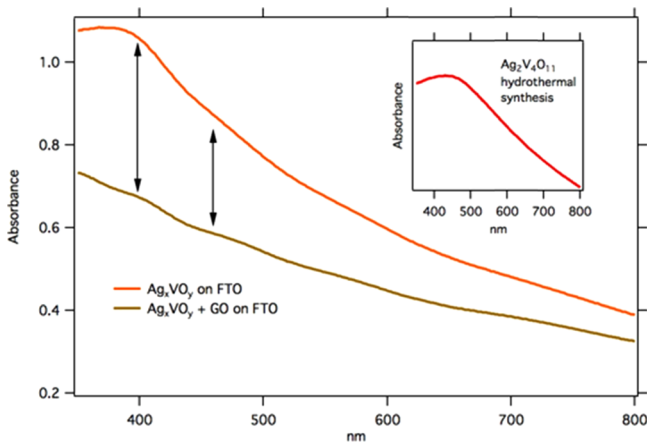**Figure 4.** UV−vis spectra of Ag_xVO_y and $Ag_xVO_y\&GO$ deposited on FTO. Both spectra have been obtained after running several CV cycles (0.0−0.9 V vs SHE) to dissolve most of the metallic Ag. The arrows indicate absorption due to Ag_xVO_y (430−450 nm) and LSPR of residual Ag NPs (400 nm). In the inset, the UV−vis spectrum of $Ag_2V_4O_{11}$ obtained by hydrothermal synthesis and drop-casting on a soda-lime glass from an ethanol suspension is reported.

resonances (LSPRs) of Ag NPs embedded in the crystalline nanostripes or needles of $Ag_2V_4O_{11}$. These resonances are typically found at about 400 nm in the case of NPs with a diameter of 30−40, whereas a shift toward a longer wavelength is characteristic of larger aggregates. The absorption maximum, at 434 nm, due to the presence of $Ag_2V_4O_{11}$ can be seen in the figure inset, where the UV−vis spectrum of $Ag_2V_4O_{11}$ obtained by hydrothermal synthesis and drop-casting on glass from an

ethanol suspension is reported.[21] It is important to highlight that the UV−vis spectra were acquired after running several cyclic voltammetry (CV) cycles (0.0−0.9 V vs SHE) to dissolve most of the metallic Ag.

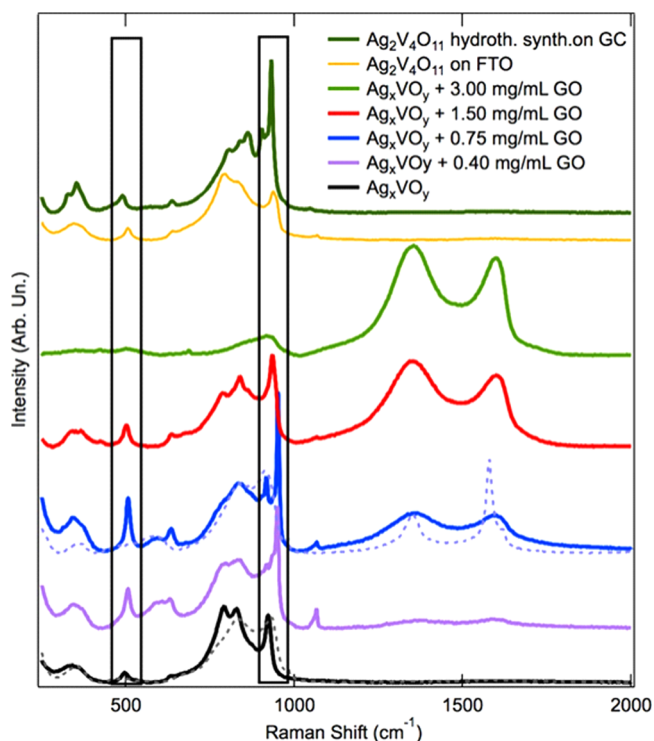In Figure 5, we report the Raman spectra obtained for samples deposited on CP and FTO using $Ag_xVO_y\&GO$

Figure 5. Raman spectra of $Ag_2V_4O_{11}$ and of samples containing $Ag_xVO_y\&GO$ with various amounts. The spectra are normalized to the intensity at 840 cm^{-1} (excluding the sample containing 1 mg/mL GO). An offset is applied to the spectra for clarity. The Raman spectra acquired after the electrochemical measurements are reported as gray dotted lines.

precursor solutions with different amounts of GO. The spectra of the samples with GO, normalized to the intensity of the peak at 840 cm^{-1} (see below), are characterized by resonance bands at about 500, 630, 790 (sh), and 840 cm^{-1},[22,23] as well as typical GO-derived D and G bands at about 1350 and 1600 cm^{-1}. The samples prepared from solutions containing 0.40 and 0.75 mg/mL GO are also characterized by a very sharp peak at 950 cm^{-1}. This last resonance seems to shift to 930 and 925 cm^{-1} in the case of samples containing 1.50 mg/mL GO and those without GO, respectively. As a reference, we also report the Raman spectrum of $Ag_2V_4O_{11}$ obtained by hydrothermal synthesis.

There is a rather reliable correlation between V−O bond distances, bond orders, and Raman stretching frequencies, as very well clarified in the literature.[24−26] The Raman spectra of α-Ag_3VO_4 characterized by one single band at about 800 cm^{-1} and that of $Ag_4V_2O_7$ by three bands at 830, 790, and 770 (sh) cm^{-1} are typical of tetrahedral and 5-fold coordinated vanadates.[14,27] In contrast, the higher number of bands found in the spectra of the deposited samples (500, 630, 790, 840, and 950 cm^{-1}) correlates well with octahedrally coordinated vanadate species. The very intense feature at 950 cm^{-1} matches nicely with a V−O distance of about 1.6 Å and a bond order of about 1.65−1.7. These bond lengths and the corresponding
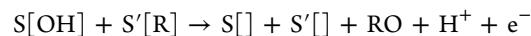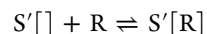
Raman frequencies are typical of octahedrally coordinated vanadium oxides containing polyanions like $V_2O_6{}^{2-}$ or $V_{10}O_{28}{}^{6-}$. In fact, there are silver vanadates, known as Ag-vanadate bronzes, that are structures deriving from β-$Ag_4V_4O_{12}$. The structure of $Ag_4V_4O_{12}$ consists of infinite chains with the formula $[V_4O_{12}]_n$.[18,28] These chains, of a zigzag shape, are double and consist of an edge sharing VO_6 distorted octahedra with the V–O bonds distributed in four domains, with the shortest one, a vanadyl bond, equal to 1.67 Å. As well described in ref 18, the conversion of β-$Ag_4V_4O_{12}$ to $Ag_xV_2O_{10}$ is possible by eliminating crystallographic shear (CS) planes of Ag_2O and O_2 according to the following reaction:

$$\beta\text{-}Ag_4V_4O_{12} \xrightarrow{-Ag_2O} Ag_2V_4O_{11} \xrightarrow{-O_2} Ag_xV_2O_{10}$$

The elimination of Ag_2O is also in agreement with the high amount of metallic Ag according to WAXD and XPS measurements, because Ag_2O can easily decompose to O_2 and Ag above 160 °C. It is worth noting that the peaks at 500 and 950 cm^{-1} together with the large structure between 750 and 880 cm^{-1} are clearly visible in the Raman spectrum of $Ag_2V_4O_{11}$ obtained by hydrothermal synthesis[10] and reported in Figure 5. Therefore, Raman spectra indicate that the deposits are mainly composed of $Ag_2V_4O_{11}$ and a smaller amount of Ag_3VO_4 (band at 790–800 cm^{-1}). The presence of a G-band at 1353 cm^{-1} and a D-band at about 1600 cm^{-1} is indicative of multilayer GO aggregates.[29] A final comment regards the spectra acquired after electrochemical measurements and therefore without the embedded metallic Ag NPs (see the following section). These spectra are reported in Figure 5 as gray dotted lines. The main difference with the spectra acquired before the electrochemical measurements is the intensity of the band at about 790 cm^{-1} in the case of the pure Ag_xVO_y sample and the intensity of the bands at 950 and 500 cm^{-1} in the case of the sample containing GO. We attribute this difference to the SERS effect due to the presence of Ag NPs. The sample containing GO also showed a pronounced leaching of the deposit as evidenced by the low intensity of the D and G bands due to GO. Finally, the Raman spectra of the deposits obtained on FTO are very similar to the ones obtained on CP (blue and dark green curves in Figure 5) and correspond to the $Ag_2V_4O_{11}$ phase.

In conclusion of the whole set of physicochemical characterizations, we have strong evidence for the prevalent presence of $Ag_2V_4O_{11}$ species in the deposited films. In the following section, we will assume such a hypothesis when discussing the PEC measurements.

Mott–Schottky Plots, PEC Measurements, and Electrochemical Sensing of Ethylenediamine. The idea behind the use of Ag-vanadates as electrochemical sensors for the detection of amines is that this material is characterized by (1) surface sites that are effective for the adsorption of N atoms through nonbonded electron pairs (Ag–O sites), (2) a certain number of surface sites at which anodic discharge of water, with the generation of OH radicals, occurs at sufficiently low overpotentials (usually metal oxides or composites of metal oxides) and a good stability at alkaline pH. The mechanism proposed in the literature for the oxidative detection of aliphatic amines, according to the above-mentioned requisites, is the following[30]

$$S[\,] + H_2O \rightarrow S[OH] + H^+ + e^-$$

$$S'[\,] + R \rightleftharpoons S'[R]$$

$$S[OH] + S'[R] \rightarrow S[\,] + S'[\,] + RO + H^+ + e^-$$

where S[OH] indicates a surface site where the anodic discharge of water occurs and S′[R] a site where ammines are adsorbed by lone-pair donation.

To these requirements, we can add that of stable n-type conductivity, so that the increase in the anodic current under illumination can improve the sensitivity. In this paragraph, we will, therefore, verify first the possibility of using this material as a photoanode with the production of a sufficiently stable photocurrent. Then, we will also consider the effect of the addition of GO on the photoactive properties of the Ag-vanadates. Finally, we will present the electrochemical detection of ethylenediamine in the dark as well as under illumination.

The Mott–Schottky plots obtained from pure Ag_xVO_y and Ag_xVO_y&GO 0.75 mg/mL samples are reported in Figure 6.
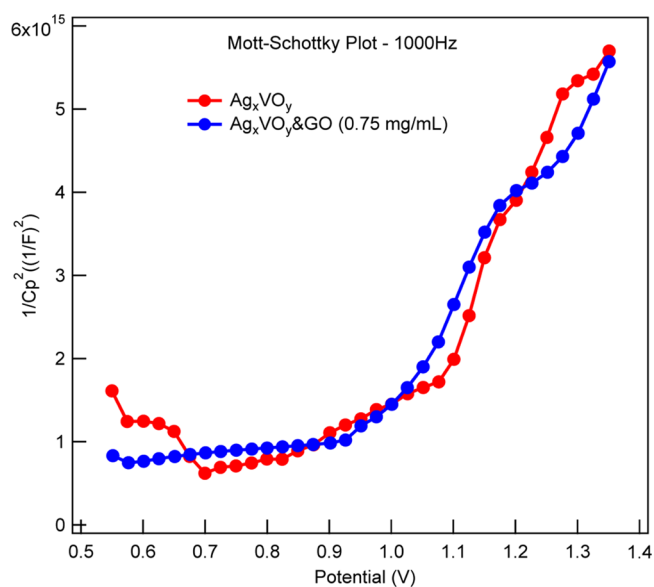

Figure 6. Mott–Schottky plots of samples obtained from Ag_xVO_y and Ag_xVO_y&GO 0.75 mg/mL solutions.

They present a typical positive slope characteristic of an n-type behavior. The imperfect linear shape of the plot might be due to the presence of different phases, as already indicated by the Raman and X-ray diffraction (XRD) data, which can provide different electronic properties in the synthesized materials under polarization conditions. The flat-band position is about 0.95 V. The n-type conductivity is somewhat surprising and opposite to what is usually expected in the case of typical photocatalysts such as Ag_3VO_4 or $Ag_4V_2O_7$. In particular, α-Ag_3VO_4, the stable phase at room temperature, is expected to be a p-type semiconductor according to the theoretical predictions and confirmed by optical and electrical measurements, because the energy of formation of oxygen vacancies is high and oxygen vacancies do not compensate for the Ag cation vacancies. As a result, holes are formed and therefore Ag-vanadates are usually characterized by a p-type conductivity.[11,31,32] Danzhen Li,[33] who synthesized $Ag_4V_2O_7$ by a hydrothermal procedure at low pH (between 4 and 6), obtained a p-type behavior as well, caused by Ag vacancies in the lattice with quite good photocatalytic performances under visible light. Mullins and co-workers prepared Ag_3VO_4 thin
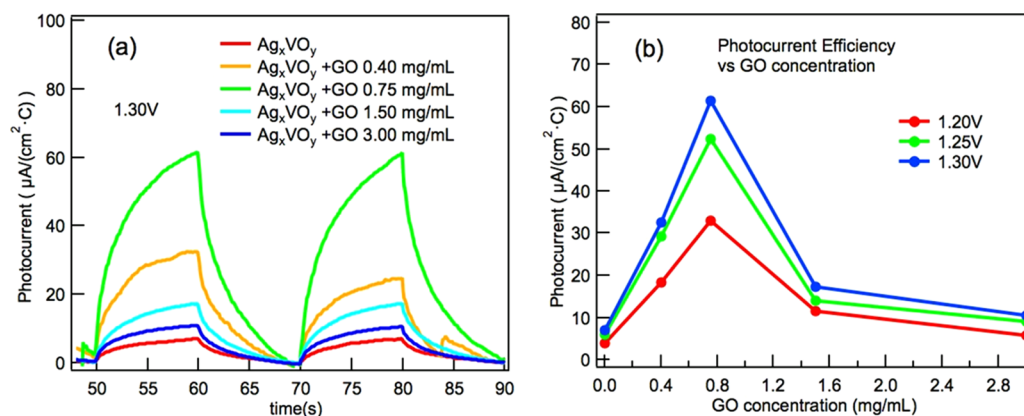
Figure 7. (a) Photocurrent of samples obtained from pure Ag$_x$VO$_y$ solution and Ag$_x$VO$_y$&GO at different concentrations at 1.3 V vs SHE. (b) Photocurrent vs GO concentrations at different voltages. The renormalized photocurrent values (see text) expressed as μA/(cm^2 mg Ag$_2$V$_4$O$_{11}$) can be obtained by multiplying for a conversion factor = 0.195 C/mg Ag$_2$V$_4$O$_{11}$ (C stays for coulomb).

films by SILAR obtaining an n-type conductivity after a mild annealing of the deposit at temperatures slightly higher than 150 °C. They measured an increase in the anodic photocurrent up to annealing temperatures of 300 °C, but with a very quick decay of it after only 30 s. This decay was also accompanied by a shift of the flat-band potential to more positive values. The authors concluded that the high values of the initial photocurrents were actually due to the removal of oxygen vacancies created by the annealing procedure.[11] An n-type conductivity was instead found in the case of Ag$_x$V$_2$O$_5$ vanadate bronzes.[34] In our case, the main component is Ag$_2$V$_4$O$_{11}$, especially in the case of samples containing GO, and we can say that this type of vanadate is characterized by an n-type conductivity and by a lower band gap (1.88−2.0 eV)[35,21] compared with the values found in the literature for Ag$_3$VO$_4$ and other vanadates (α-Ag$_3$VO$_4$: 2.4−2.2 eV; β-Ag$_3$VO$_4$: 2.67 eV; Ag$_4$V$_2$O$_7$: 2.4 eV; and AgVO$_3$: 2.5 eV).[4,36]

In Figure 7, we report typical photocurrent responses of samples obtained from Ag$_x$VO$_y$ and Ag$_x$VO$_y$&GO with increasing amounts of GO. All of the samples are characterized by an n-type conductivity, and the obtained current density values in a 0.1 M KHCO$_3$ solution (pH = 8.3) are all between about 60 and 20 μA/cm^2 at 1.30 V versus SHE with the onset just below 1.20 V, as reported in Figure 7.

The rather slow increase of the photocurrent by illuminating the sample is due to the morphology of the deposit on the CP, which is also found in other cases.[37] In any case, the addition of 0.25 mL of pure methanol in the electrolytic solution (total volume 50 mL) did not show any clear increase of the photocurrent and therefore we think that the hole mobility is rather small, as already verified by Mullins and co-workers.[11] The effect of the addition of GO to the precursor solution was verified by normalizing the photocurrent (recorded at 1.20, 1.25, and 1.30 V vs SHE) to the amount of Ag (as Ag$^+$ in the vanadate) contained in each sample. The amount of Ag$^+$, after stripping the metallic Ag by applying several CV cycles between 0.0 and 0.9 V, was obtained dissolving the deposit by dropping a concentrated NH$_3$ solution ($\approx$1 mL) on the CP filter and rinsing with 50 mL of 0.1 M KHCO$_3$ solution. The same solution was then used to redeposit metallic Ag NPs on a new CP filter and finally re-dissolving them by performing a CV between 0.0 and 0.9 V. This procedure allows only the determination of a charge proportional to the amount of Ag$^+$ in the sample. It is also important to notice that the amount of

metallic Ag contained in the deposit, as shown by XPS and WAXD measurements, is completely dissolved as soon as potentials above 0.5 V versus SHE are applied. To be sure that each sample was free from metallic Ag, several CV cycles were performed (between 0.0 and 0.9 V) before photocurrent determination. Under these conditions, with a pH solution of 8.3, no precipitation of Ag$_2$O or Ag$_2$CO$_3$ on the carbon fibers can occur.[a] In conclusion, the amount of Ag$^+$ determined as described above corresponds only to the Ag$^+$ ions contained in the vanadate. The results of this normalization procedure are reported in Figure 7, wherein it is clear that the best compromise is obtained by using the solution containing 0.75 mg/mL of GO.

The effect of GO on the charge transfer resistance at the electrolyte/electrode interface can be evaluated by electrochemical impedance spectroscopy (EIS) measurements obtained on a pure Ag$_x$VO$_y$ sample and on the one containing 0.75 mg/mL of GO. The Nyquist plots reported in Figure 8 indicate that, apart from the lower resistance of the sample containing GO, the pure Ag$_x$VO$_y$ has a capacitive behavior with a very high resistance.

In Figure 9, we show the Bode plot obtained from 10^4 to 10^{-1} Hz. The EIS spectra show two time constants, differing in the frequency domain, wherein higher frequencies can be assigned to the double-layer capacitance/charge transfer resistance system, in series with a capacitance/resistance corresponding with the electronic transfer of a thicker inner layer. It is evident that the polarization resistance of the sample containing GO is about two-thirds of that containing pure Ag$_x$VO$_y$ (resistance extracted from the Bode plot at the lowest frequency).

We have simulated the EIS measurements with equivalent circuits, as reported in Figure 9. In the simulation, R_0 represents the solution resistance. Y_1 and R_1 represent the charge transfer process between the film and the electrolyte within the double layer on the electrode, whereas Y_2 and R_2 represent the capacity and resistance of the film. In both time constants, capacitances were substituted by constant phase elements (CPEs). To take into account their nonideal character,[38] the Brug equation[39] was used to convert CPE into capacitances. The obtained values are, in the case of the pure oxide: C_{film} = 1.97 mF, C_{DL} = 215 μF, whereas in the case of the Ag$_x$VO$_y$&GO composite: C_{film} = 398 μF, C_{DL} = 485 μF. The film resistance (R_2) reduces from 130 to 28 kΩ after the introduction of GO. Therefore, the

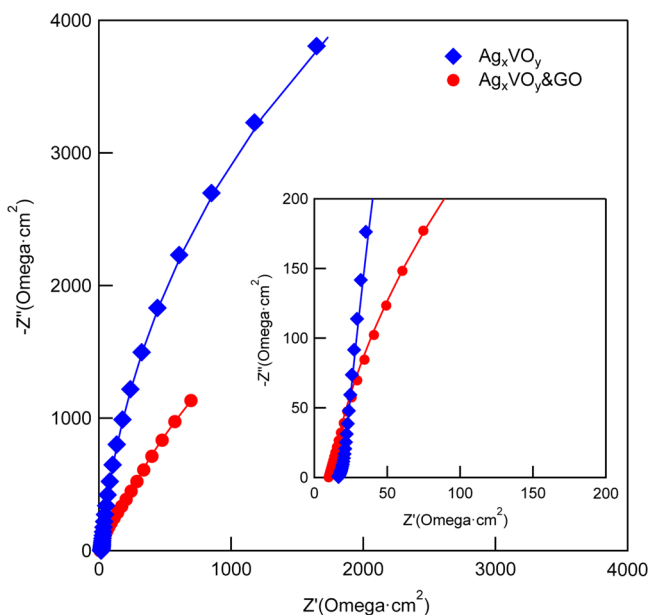**Figure 8.** Fitted Nyquist plots of the samples prepared from pure Ag_xVO_y solution and Ag_xVO_y&GO 0.75 mg/mL.

better performance in terms of electronic transfer obtained for the samples containing GO can be associated with a better electrical conductivity of the deposit that shows the presence of a higher amount of $Ag_2V_4O_{11}$, characterized by n-type electrical conductivity,[28] as indicated by Raman and XRD spectra. For now, we can simply associate a lower resistance and a more efficient charge injection on the electrode surface with the presence of GO. It is worth pointing out that the two best performing samples are those that, according to Raman spectra

and XRD, show also the highest amount of $Ag_2V_4O_{11}$, whereas samples containing 1.5 and 3 mg/mL GO present a less intense band at 950 cm^{-1}, which we consider as representative of the presence of short V−O bonds. Therefore, it appears that a proper ratio between GO and Ag_xVO_y/NH$_3$ solution is crucial in favoring the formation of these compounds. To our best knowledge, in the literature there is another example of composite Ag_xVO_4&GO obtained by simply mixing preformed Ag_3VO_4 and GO, which does not show the formation of any $Ag_2V_4O_{11}$ phase.[14]

As stated in the introduction, $Ag_2V_4O_{11}$ is a versatile vanadate and its use as a sensor in the detection of amines and ethanol in the gas phase has already been tested.[10] The detection of amines in a water solution, especially biogenic amines, is also an important task. The detection of biogenic amines and, in particular, histamine by electrochemical methods requires the use of polycrystalline boron-doped diamond thin-film electrodes, gold nanocrystal-modified glassy carbon electrodes, or thin-film Ni electrodes, as described in refs 40, 41. In our case, the electrode can be prepared in a few minutes and therefore can be considered as an interesting alternative to the methods mentioned above. Ethylenediamine (EDA) is chemically similar to biogenic amines but easier to handle and can be used as a tester for biogenic amines.

In Figure 10, we show the response of the Ag_xVO_y/CP sample to the addition of small amounts (200 μL) of 0.01 M EDA solution in 0.1 M KHCO$_3$, by reporting the current at 1.15 V versus SHE (the peak corresponds to the oxidation of the amine[41,42]) as a function of the EDA concentration. The electrode showed a good sensitivity to the addition of EDA with a linear range between about 50 and 300 μm concentrations. The detection limit, calculated in the response linear range, considering ΔI as 3 times the standard deviation in
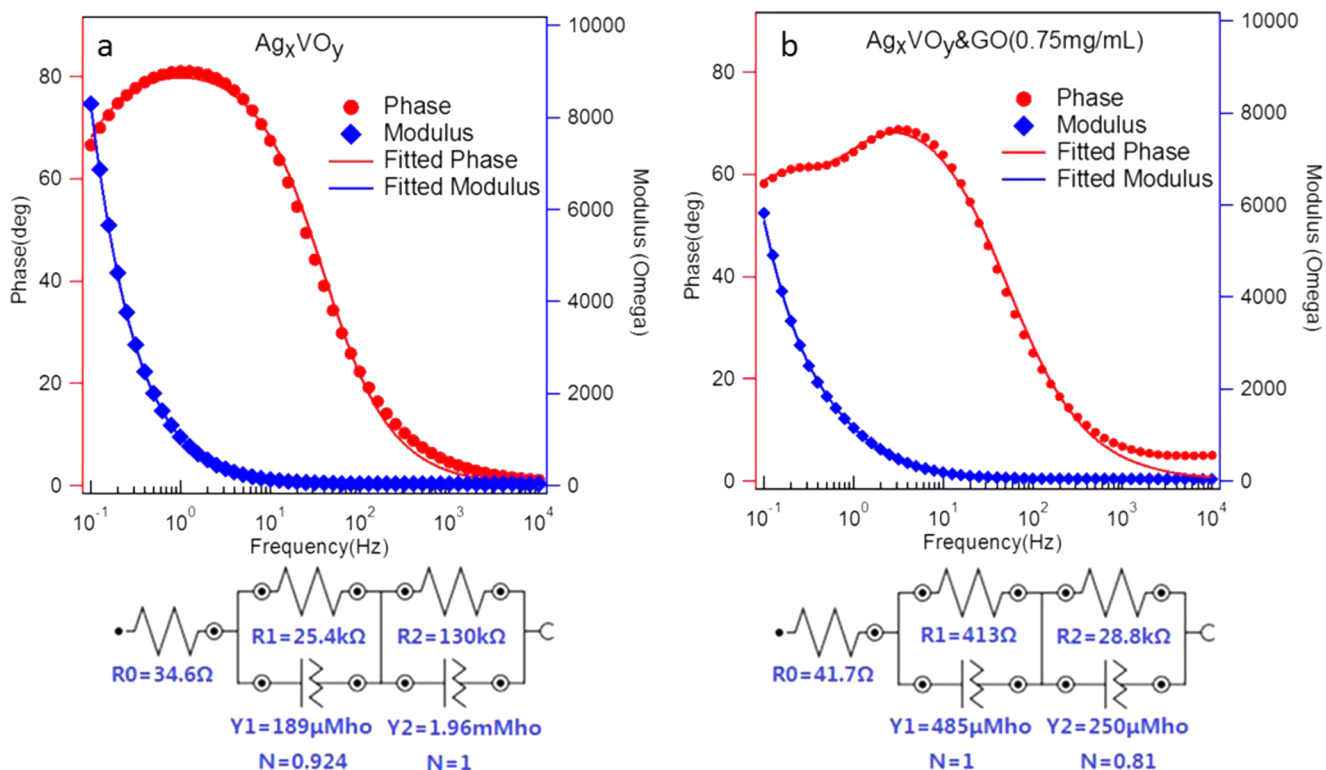

Figure 9. Simulated EIS spectrum of the samples prepared from Ag_xVO_y, (a) and Ag_xVO_y&GO 0.75 mg/mL (b) and simulation models.
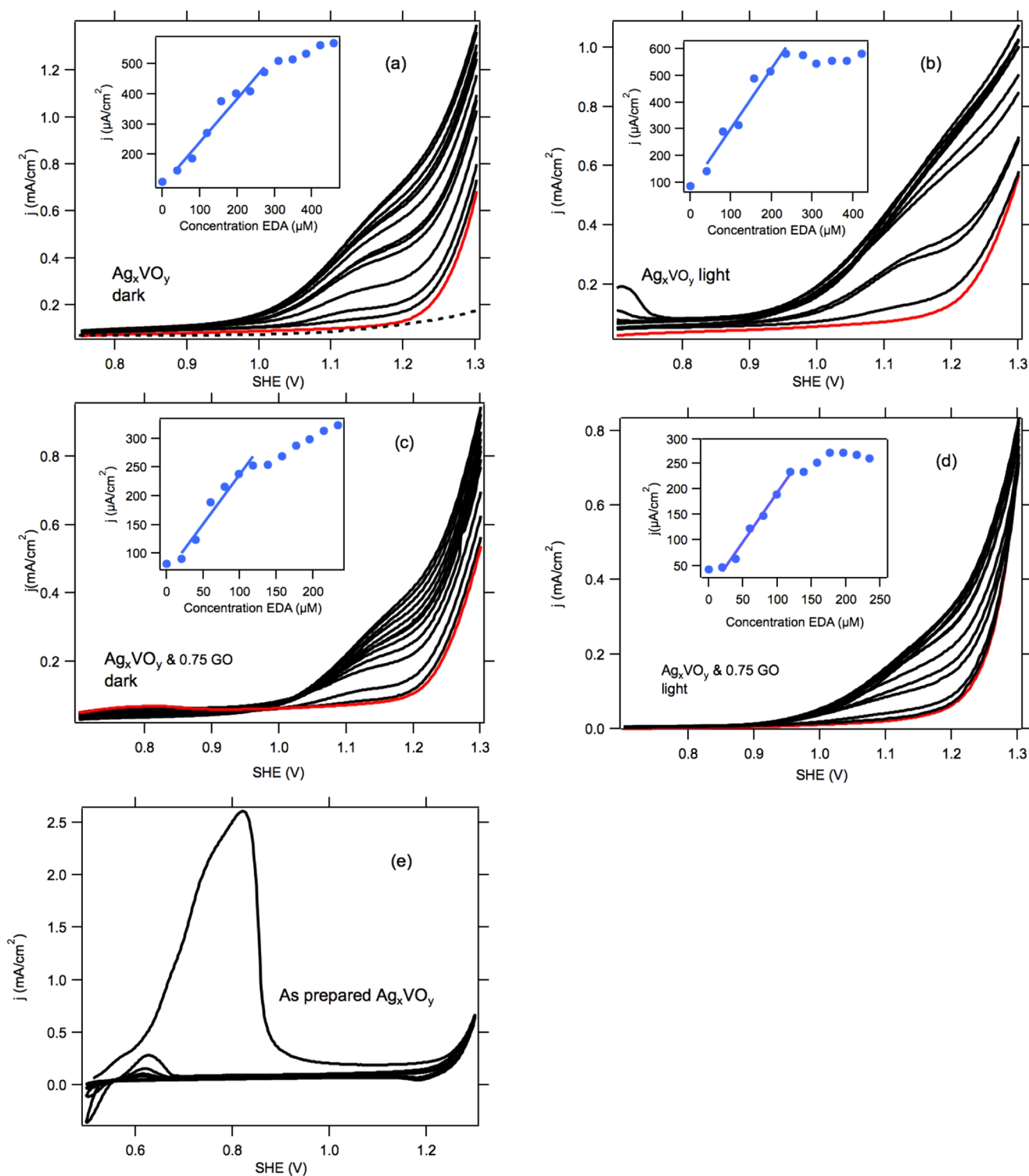
Figure 10. (a) Ag_xVO_y electrode response to the addition of 200 μL of 0.01 M EDA solution. (b) Ag_xVO_y response to the addition of 200 μL of 0.01 M EDA solution under illumination. (c) Ag_xVO_y&GO 0.75 mg/mL response to the addition of 100 μL of 0.01 M EDA solution. (d) Ag_xVO_y&GO 0.75 mg/mL response to the addition of 100 μL of 0.01 M EDA solution under illumination. The current values at 1.15 V vs SHE are reported in the figure insets as a function of the EDA concentration. The bottom LVS curve (red) is the electrode response before EDA addition. The calculated detection limit, considering $\Delta I = 3\sigma$, where σ is the standard deviation calculated in the nonfaradic region, is 0.2 ppm in the case of Ag_xVO_y. The dotted curve (a) is the response of a clean CP electrode in the same solution after 10 EDA additions (3.8×10^{-4} M). (e) CV on a freshly prepared Ag_xVO_y sample in $KHCO_3$ solution.

the nonfaradic region, was about 0.2 ppm. This value is comparable to other literature data.[40,43] Slightly worse results are obtained for the nanocomposite with GO (Figure 10c). In this case, the linear range is also lower than in the case of

Ag_xVO_y as well as the detection limit. This behavior indicates that the linear range and the response of the electrode strongly depend on the amount of the deposited catalyst (the amount of Ag_xVO_y is less in the case of samples containing GO, as

discussed above in this section) and possibly by the presence of GO sheets, which prevents the adsorption of the amines on the vanadate surface.

It must be noted that before performing a sensing measurement, each electrode must be "activated" by applying some CV cycles between 0.0 and 0.9 V versus SHE to strip the amount of metallic Ag (in the form of Ag NPs) that forms during the deposition process (see XRD and XPS characterization) and after exposure of the electrode to light for a few hours. The accumulation of Ag NPs on the surface of Ag-vanadates is well documented and was observed also in the case of $Ag_2V_4O_{11}$ crystals by HR-TEM measurements.[17] Considering the good photoactivity of the films, as described in the previous part of this section (n-type behavior and stable photocurrents up to 1.30 V vs SHE), we carried out the sensing experiments also on a Ag_xVO_y film under illumination (Figure 10b). As clearly visible from Figure 10b, when the sensing is performed under illumination, the increase in the anodic current (the onset of the photocurrent is above 1.0 V) corresponds to a higher slope of the linear range of the electrode, and this allows a lower detection limit (≈ 0.1 ppm). The linear range is slightly lower than that in the previous case probably because of the formation of Ag NPs induced by the light as testified by the appearance of a weak anodic current at about 0.65 V (Figure 10b). As mentioned above, although the presence of GO improves the photocurrent values, considering the value normalized to the Ag-vanadate content, the sensing efficiency depends instead on the absolute amount of Ag-vanadate and therefore when the sensing experiment is performed using the Ag_xVO_y&GO 0.75 mg/mL sample (Figure 10d), the performances are only slightly better than those obtained under dark conditions (higher slope value in the linear range) and in any case comparable to those obtained with the pure Ag_xVO_y sample in the dark.

CONCLUSIONS

A quick and easy synthesis of Ag_xVO_y and Ag_xVO_y/GO thin films or nanoaggregates was obtained by aerosol-assisted deposition. The deposition process that allows us to obtain a ready-to-work electrode can be completed in a few minutes, at difference with the more standard, hydrothermal synthesis, which requires a heat treatment in a closed vessel at 180 °C for about 48 h. The obtained deposit adheres well on CP or FTO and does not require the addition of nafion to prevent material loss during the electrochemical measurements. The precursor solution consisted of an alkaline solution (NH_4OH) containing Ag, V, and O with a Ag/V atomic ratio of 3:1. Different amounts of GO flakes were added to the precursor solution to study the effect of GO on the physicochemical and electrochemical properties of the Ag-vanadate film.
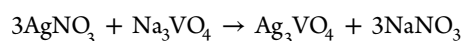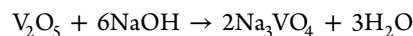
The sample prepared without GO consisted of a mix of $Ag_2V_4O_{11}$ and α-Ag_3VO_4 phases with a large particle size distribution. The addition of GO resulted in a significant increase of the $Ag_2V_4O_{11}/\alpha$-Ag_3VO_4 ratio and a more homogeneous dispersion of the $Ag_2V_4O_{11}$ nanoparticles on the GO sheets. This material was characterized by a stable n-type conductivity. The presence of GO led to the improvement of the electrical conductivity of the film by assisting the electron injection on the electrode surface.

The Ag_xVO_y samples deposited on CP without and with GO were finally tested as electrochemical sensors for amine detection in solution. The electrodes showed a good sensitivity to the amine with a linear range between about 50 to 300 μm

concentrations and with a detection limit of about 0.2 ppm. A lower detection limit could be obtained by performing the sensing measurements under illumination.

EXPERIMENTAL SECTION

Aerosol-Assisted Deposition. The precursor solution containing Ag, V, and O in the stoichiometric amount (3Ag/ V), named throughout the text as Ag_xVO_y solution, was prepared according to the following reactions:

$$V_2O_5 + 6NaOH \rightarrow 2Na_3VO_4 + 3H_2O$$

$$3AgNO_3 + Na_3VO_4 \rightarrow Ag_3VO_4 + 3NaNO_3$$

V_2O_5 (4.0269 g, 22.1 mmol) and NaOH (5.3137 g, 133 mmol) were dissolved in deionized (DI) water (15 mL) to obtain a Na_3VO_4 solution. $AgNO_3$ (22.5581 g, 133 mmol) was dissolved in water (20 mL). Then, both solutions were mixed together and stirred for 15 min to induce the precipitation of Ag_3VO_4 (or other Ag-vanadates). Finally, a concentrated (35% weight) NH_4OH solution was added dropwise until a clear solution (Ag_xVO_y, 100 mg/mL) was obtained. Lyophilized GO obtained by the Hummers method was dissolved in milli-Q water to obtain a solution with a concentration of 2 mg/mL. Then, 5 Ag_xVO_y solutions (5.0 mg/mL) with variable GO contents (0, 0.40, 0.75, 1.50, and 3.00 mg/mL) were prepared (Ag_xVO_y&GO).

A commercial medical ultrasonic aerosol generator was used to deposit the composite on a 15 mm round CP (Toray, TGP-H-60) or on FTO (Aldrich, 7 Ω/sq). Volumes of 4 mL of the Ag_xVO_y&GO solutions and 2 mL of concentrated NH_4OH were mixed together and then introduced in the aerosol generator. The resulting vapor was directed by an air stream (flow rate = 60 mL/min) on the CP substrate, which was kept at 250 °C throughout the deposition. The samples were named Ag_xVO_y, Ag_xVO_y&GO 0.4 mg/mL, Ag_xVO_y&GO 0.75 mg/mL, Ag_xVO_y&GO 1.50 mg/mL, and Ag_xVO_y&GO 3.00 mg/mL according to the content of GO in the precursor solution. The procedure followed to deposit Ag_xVO_y and Ag_xVO_y&GO on FTO was the same but the substrate was kept at 270 °C.

Material Characterization. The nano- and micro-scale morphology of the materials was studied by field electron gun (FEG) SEM, using a Zeiss Supra 35 VP equipment. Micrographs were taken with an acceleration voltage of 5 kV and using an in-lens high-resolution detector. EDX analysis was performed on the same machine with an accelerating voltage of 10 kV. For TEM analysis, the samples were embedded in acrylic resin LRW and allowed to polymerize O.N. at 60 °C. The samples were cut with an LKB ultramicrotome, and 100 nm thick slices were deposited on 200 mesh copper grids. The observation was made by a TEM FEI Tecnai G12 operating at 100 kV. The images were acquired with an OSIS Veleta camera.

XPS measurements were performed on a custom-built UHV chamber (base pressure = 5×10^{-10} mbar) equipped with a nonmonochromatized double-anode X-ray source (Omicron DAR-400), a hemispherical electron analyzer (Omicron EA-125), and a 5-channeltrons detection assembly. The electron analyzer acceptance angle was $\pm$ 4°, and the diameter of the analyzed area was 3 mm. The spectra were acquired with Al Kα radiation. The binding energy scale was calibrated with respect to the Pt 4f$_{7/2}$, and all reported spectra intensities were obtained after a Shirley background subtraction.

WAXD patterns were recorded in the diffraction angular range of 10–50° 2θ by a Philips X'Pert PRO diffractometer,

working in the reflection geometry and equipped with a graphite monochromator on the diffracted beam (Cu Kα radiation)

Raman spectra were acquired with a ThermoFisher DXR Raman microscope using a 532 nm laser (5 mW), focused on the sample with a 50× objective (Olympus) obtaining a spot size of about 1 μm. UV−vis spectra were acquired in the absorbance mode on a UV−vis Cary 5E spectrophotometer.

All of the electrochemical measurements were obtained in 0.1 M KHCO$_3$ solution in a three-electrode electrochemical cell controlled by Autolab PGSTAT204. The Pt electrode and saturated calomel electrode (SCE) were used as the counter electrode and reference electrode, respectively. PEC measurements were done by visible light LED sources controlled by the optical bench (Metrohm-Autolab) coupled to the Autolab PGSTAT204. All of the potentials mentioned in this article are referred to the standard hydrogen electrode (SHE). EIS data were obtained at the open circuit potential of the samples in the cell without light. The amplitude for EIS measurements is ±10 mV, and the frequency range was set from 10^4 to 10^{-1} Hz performing 10 points per decade. Stability tests (1 h) were conducted by setting the potential from 0.55 to 1.30 V with linear steps of 50 mV under visible light illumination. Then, the values at 1.20−1.30 V were collected to estimate the stability of the prepared samples. The electrochemical detection of EDA was performed in a 0.1 M KHCO$_3$ solution by linear sweep voltammetry scans with several additions of 200 μL of 0.01 M EDA solutions and using an SCE reference electrode and a glassy carbon counter electrode to prevent eventual dissolution of Pt and redeposition of Pt NPs on the working electrode.[44] The scan rate was 0.05 V/s.

AUTHOR INFORMATION

Corresponding Author

*E-mail: gianandrea.rizzi@unipd.it.

ORCID

Laura Calvillo: 0000-0001-9256-0133
Stefano Agnoli: 0000-0001-5204-5460
Gian Andrea Rizzi: 0000-0001-5201-8104
Gaetano Granozzi: 0000-0002-9509-6142

Present Address

$^{\parallel}$Department of Chemistry, University of Oslo, Sem Sælands vei 26, 0371 Oslo, Norway (J.Z.).

Notes

The authors declare no competing financial interest.

ACKNOWLEDGMENTS

ADDITIONAL NOTE

^{a}In a 0.1 M KHCO$_3$ solution (pH = 8.3), where the CO$_3^{2-}$ concentration is about 10^{-3} M, the precipitation of Ag$_2$CO$_3$ occurs for [Ag$^+$] higher than 10^{-4} M. The stripping of metallic Ag, as deduced from the CV data, always leads to [Ag$^+$] $\leq$ 6 × 10^{-6} M. Similar considerations can be applied considering the formation of Ag(OH) and Ag$_2$O.

REFERENCES

(1) Dinnebier, R. E.; Kowalevsky, A.; Reichert, H.; Jansen, M. Polymorphism of Ag$_3$VO$_4$. *Z. Kristallogr.* **2007**, *222*, 420−426.

(2) Gelderman, K.; Lee, L.; Donne, S. W. Flat-Band Potential of a Semiconductor: Using the Mott−Schottky Equation. *J. Chem. Educ.* **2007**, *84*, 685.

(3) Luster, B.; Stone, D.; Singh, D. P.; to Baben, M.; Schneider, J. M.; Polychronopoulou, K.; Rebholz, C.; Kohli, P.; Aouadi, S. M. Textured VN coatings with Ag3VO4 solid lubricant reservoirs. *Surf. Coat. Technol.* **2011**, *206*, 1932−1935.

(4) Cloet, V.; Raw, A.; Poeppelmeier, K. R.; Trimarchi, G.; Peng, H.; Im, J.; Freeman, A. J.; Perry, N. H.; Mason, T. O.; Zakutayev, A.; Ndione, P. F.; Ginley, D. S.; Perkins, J. D. Structural, Optical, and Transport Properties of α- and β-Ag$_3$VO$_4$. *Chem. Mater.* **2012**, *24*, 3346−3354.

(5) Han, C.; Pi, Y.; An, Q.; Mai, L.; Xie, J.; Xu, X.; Xu, L.; Zhao, Y.; Niu, C.; Khan, A. M.; He, X. Substrate-Assisted Self-Organization of Radial β-AgVO$_3$ Nanowire Clusters for High Rate Rechargeable Lithium Batteries. *Nano Lett.* **2012**, *12*, 4668−4673.

(6) Li, D.; Duan, X.; Qin, Q.; Fan, H.; Zheng, W. Facile synthesis of novel alpha-Ag3VO4 nanostructures with enhanced photocatalytic activity. *CrystEngComm* **2013**, *15*, 8933−8936.

(7) Wang, J.; Wang, P.; Cao, Y.; Chen, J.; Li, W.; Shao, Y.; Zheng, Y.; Li, D. A high efficient photocatalyst Ag3VO4/TiO2/graphene nanocomposite with wide spectral response. *Appl. Catal., B* **2013**, *136−137*, 94−102.

(8) Zheng, J.; Calvillo, L.; Rizzi, G. A.; Granozzi, G. VO$_2$/V$_2$O$_5$:Ag Nanostructures on a DVD as Photoelectrochemical Sensors. *ChemPlusChem* **2016**, *81*, 391−398.

(9) Chen, Z. J.; Gao, S. K.; Li, R. H.; Wei, M.; Wei, K.; Zhou, H. S. Lithium insertion in ultra-thin nanobelts of Ag$_2$V$_4$O$_{11}$/Ag. *Electrochim. Acta* **2008**, *53*, 8134−8137.

(10) Fu, H. T.; Yang, X. H.; Jiang, X. C.; Yu, A. B. Silver vanadate nanobelts: A highly sensitive material towards organic amines. *Sens. Actuators, B* **2014**, *203*, 705−711.

(11) Chemelewski, W. D.; Mabayoje, O.; Mullins, C. B. SILAR Growth of Ag3VO4 and Characterization for Photoelectrochemical Water Oxidation. *J. Phys. Chem. C* **2015**, *119*, 26803−26808.

(12) Zanatta, M.; Calvillo, L.; Zheng, J.; Rizzi, G. A.; Durante, C.; Giallongo, G.; Chirkov, D.; Colazzo, L.; Marega, C.; Gennaro, A.; Granozzi, G. Cu$_2$O/TiO$_2$ heterostructures on a DVD as easy & cheap photoelectrochemical sensors. *Thin Solid Films* **2016**, *603*, 193−201.

(13) Min, Z.; Wen-Long, W.; Xue-Dong, B. Preparing three-dimensional graphene architectures: Review of recent developments. *Chin. Phys. B* **2013**, *22*, No. 098105.

(14) Das, D. P.; Barik, R. K.; Das, J.; Mohapatra, P.; Parida, K. M. Visible light induced photo-hydroxylation of phenol to catechol over RGO-Ag$_3$VO$_4$ nanocomposites without the use of H$_2$O$_2$. *RSC Adv.* **2012**, *2*, 7377−7379.

(15) Mohandes, F.; Salavati-Niasari, M. Sonochemical synthesis of silver vanadium oxide micro/nanorods: Solvent and surfactant effects. *Ultrason. Sonochem.* **2013**, *20*, 354−365.

(16) Wang, D. S.; Duan, Y. D.; Luo, Q. Z.; Li, X. Y.; An, J.; Bao, L. L.; Shi, L. Novel preparation method for a new visible light photocatalyst: mesoporous TiO$_2$ supported Ag/AgBr. *J. Mater. Chem.* **2012**, *22*, 4847−4854.

(17) Zandbergen, H. W.; Crespi, A. M.; Skarstad, P. M.; Vente, J. F. 2 Structures of Ag2-Xv4o11, Determined by High-Resolution Electron-Microscopy. *J. Solid State Chem.* **1994**, *110*, 167−175.

(18) Rozier, P.; Savariault, J. M.; Galy, J. beta AgVO3 crystal structure and relationships with Ag2V4O11 and delta AgxV2O5. *J. Solid State Chem.* **1996**, *122*, 303−308.

(19) Klug, H. P.; Alexander, L. E. *X-ray Diffraction Procedures for Polycrystalline and Amorphous Materials*, 2nd ed.; Wiley: New York, 1974, p xxv.

(20) Hindeleh, A. M.; Johnson, D. J. The resolution of multipeak data in fibre science. *J. Phys. D: Appl. Phys.* **1971**, *4*, 259−263.

(21) Shi, H. F.; Li, Z. S.; Kou, J. H.; Ye, J. H.; Zou, Z. G. Facile Synthesis of Single-Crystalline Ag2V4O11 Nanotube Material as a Novel Visible-Light-Sensitive Photocatalyst. *J. Phys. Chem. C* **2011**, *115*, 145−151.

(22) Cattelan, M.; Agnoli, S.; Favaro, M.; Garoli, D.; Romanato, F.; Meneghetti, M.; Barinov, A.; Dudin, P.; Granozzi, G. Microscopic view on a chemical vapor deposition route to boron-doped graphene nanostructures. *Chem. Mater.* **2013**, *25*, 1490−1495.

(23) Zhu, Y.; Murali, S.; Cai, W.; Li, X.; Suk, J. W.; Potts, J. R.; Ruoff, R. S. Graphene and Graphene Oxide: Synthesis, Properties, and Applications. *Adv. Mater.* **2010**, *22*, 3906−3924.

(24) Wachs, I. E.; Weckhuysen, B. M. Structure and reactivity of surface vanadium oxide species on oxide supports. *Appl. Catal., A* **1997**, *157*, 67−90.

(25) Wachs, I. E.; Briand, L. E.; Jehng, J.-M.; Burcham, L.; Gao, X. Molecular structure and reactivity of the group V metal oxides. *Catal. Today* **2000**, *57*, 323−330.

(26) Hardcastle, F. D.; Wachs, I. E. Determination of vanadium-oxygen bond distances and bond orders by Raman spectroscopy. *J. Phys. Chem.* **1991**, *95*, 5031−5041.

(27) de Oliveira, R. C.; Gracia, L.; Assis, M.; Li, M. S.; Andres, J.; Longo, E.; Cavalcante, L. S. Disclosing the electronic structure and optical properties of Ag4V2O7 crystals: experimental and theoretical insights. *CrystEngComm* **2016**, *18*, 6483−6491.

(28) Takeuchi, K. J.; Marschilok, A. C.; Davis, S. M.; Leising, R. A.; Takeuchi, E. S. Silver vanadium oxides and related battery applications. *Coord. Chem. Rev.* **2001**, *219*, 283−310.

(29) Favaro, M.; Carraro, F.; Cattelan, M.; Colazzo, L.; Durante, C.; Sambi, M.; Gennaro, A.; Agnoli, S.; Granozzi, G. Multiple doping of graphene oxide foams and quantum dots: new switchable systems for oxygen reduction and water remediation. *J. Mater. Chem. A* **2015**, *3*, 14334−14347.

(30) Ge, J. S.; Johnson, D. C. Electrocatalysis of Anodic Oxygen-Transfer Reactions - Aliphatic-Amines at Mixed Silver-Lead Oxide-Film Electrodes. *J. Electrochem. Soc.* **1995**, *142*, 1525−1531.

(31) Wang, S.; Li, D.; Sun, C.; Yang, S.; Guan, Y.; He, H. Synthesis and characterization of g-C3N4/Ag3VO4 composites with significantly enhanced visible-light photocatalytic activity for triphenylmethane dye degradation. *Appl. Catal., B* **2014**, *144*, 885−892.

(32) Sivakumar, V.; Suresh, R.; Giribabu, K.; Narayanan, V. AgVO3 nanorods: Synthesis, characterization and visible light photocatalytic activity. *Solid State Sci.* **2015**, *39*, 34−39.

(33) Wang, J.; Yang, X.; Chen, J.; Xian, J.; Meng, S.; Zheng, Y.; Shao, Y.; Li, D. Photocatalytic Activity of Novel Ag4V2O7 Photocatalyst Under Visible Light Irradiation. *J. Am. Ceram. Soc.* **2014**, *97*, 267−274.

(34) Liang, Y.; Zhu, L. F.; Liu, P.; Li, H. B.; Xiao, J.; Ji, X. W.; Yang, G. W. Ag2V4O11 nanostructures for highly ethanol sensitive performance. *CrystEngComm* **2013**, *15*, 6131−6135.

(35) Ju, P.; Fan, H.; Ai, S. Y.; Zhang, D.; Wang, Y. Photocatalytic activity of one-dimensional Ag2V4O11 nanowires in the degradation of bisphenol a under visible-light irradiation. *Res. Chem. Intermed.* **2015**, *41*, 3683−3697.

(36) Konta, R.; Kato, H.; Kobayashi, H.; Kudo, A. Photophysical properties and photocatalytic activities under visible light irradiation of silver vanadates. *Phys. Chem. Chem. Phys.* **2003**, *5*, 3061−3065.

(37) Carraro, F.; Calvillo, L.; Cattelan, M.; Favaro, M.; Righetto, M.; Nappini, S.; Pis, I.; Celorrio, V.; Fermin, D. J.; Martucci, A.; Agnoli, S.; Granozzi, G. Fast One-Pot Synthesis of MoS2/Crumpled Graphene p-n Nanonjunctions for Enhanced Photoelectrochemical Hydrogen Production. *ACS Appl. Mater. Interfaces* **2015**, *7*, 25685−25692.

(38) Growcock, F. B.; Jasinski, R. J. Time-Resolved Impedance Spectroscopy of Mild Steel in Concentrated Hydrochloric Acid. *J. Electrochem. Soc.* **1989**, *136*, 2310−2314.

(39) Brug, G. J.; van den Eeden, A. L. G.; Sluyters-Rehbach, M.; Sluyters, J. H. The analysis of electrode impedances complicated by the presence of a constant phase element. *J. Electroanal. Chem. Interfacial Electrochem.* **1984**, *176*, 275−295.

(40) Moretto, L. M.; Kalcher, K. *Environmental Analysis by Electrochemical Sensors and Biosensors*; Springer: New York, 2014; Vol. 1.

(41) Koppang, M. D.; Witek, M.; Blau, J.; Swain, G. M. Electrochemical oxidation of polyamines at diamond thin-film electrodes. *Anal. Chem.* **1999**, *71*, 1188−1195.

(42) Sarada, B. V.; Rao, T. N.; Tryk, D. A.; Fujishima, A. Electrochemical oxidation of histamine and serotonin at highly boron doped diamond electrodes. *Anal. Chem.* **2000**, *72*, 1632−1638.

(43) Raible, I.; Burghard, M.; Schlecht, U.; Yasuda, A.; Vossmeyer, T. V2O5 nanofibres: novel gas sensors with extremely high sensitivity and selectivity to amines. *Sens. Actuators, B* **2005**, *106*, 730−735.

(44) Cherevko, S.; Zeradjanin, A. R.; Topalov, A. A.; Kulyk, N.; Katsounaros, I.; Mayrhofer, K. J. J. Dissolution of Noble Metals during Oxygen Evolution in Acidic Media. *ChemCatChem* **2014**, *6*, 2219−2223.